2.1 Overview

In order to achieve the mentioned objectives in previous chapter, it is necessary to synthesize various rare earth doped $SrTiO_3$ system and characterized them for the further analysis. In this chapter, synthesis techniques of the materials and their characterizations by different instruments along with the necessary theoretical background of the various structural and electrical parameters have been described. In the present work, proposed various compositions were prepared by solid state reaction (SSR) and chemical reaction (CR) routes. Prepared compositions were investigated to characterize their structural, microstructural, chemical and electrical properties.

This chapter is shared out three proper sections. The first section is preparation and processing techniques that are involved in samples synthesis. The second section spatially highlights for different characterization techniques like structural (XRD), microstructural (FESEM), chemical (XPS) and electrical properties (Impedance spectroscopy) which are used in studies for proposed work. Thereafter third section introduces analysis techniques like X-ray Rietveld refinement, electrical conductivity and impedance spectroscopy. The experimental techniques adopted the development of anode for IT-SOFCs and analysis of rare earth doped (La^{3+}, Y^{3+}, Sm^{3+} and Dy^{3+}) $SrTiO_3$ electro-ceramic perovskite systems which are illustrated as following compositions.

(a) La-doped $SrTiO_3$ System ($La_xSr_{1-x}TiO_{3-\delta}$ where x = 0, 0.1, 0.2, 0.3 and 0.4) by SSR.

(b) Y-doped $SrTiO_3$ System ($Y_xSr_{1-x}TiO_{3-\delta}$ where x = 0, 0.03, 0.05, 0.08 and 0.1) by CR.

(c) Sm-doped $SrTiO_3$ System ($Sm_xSr_{1-x}TiO_{3-\delta}$ where x = 0.05, 0.15, and 0.2) by CR.

(d) Dy-doped $SrTiO_3$ System ($Dy_xSr_{1-x}TiO_{3-\delta}$ where x = 0.03, 0.05, 0.08 and 0.1) by CR.

2.2 Synthesis and Characterization Techniques

For synthesis of a variety of compositions of high purity raw materials viz.: strontium oxide, titanium oxide, lanthanum oxide, yttrium oxide, samarium oxide, dysprosium oxide, titanium iso-propoxide, ethylene glycol, nitric acid and citric acid have been used. The specifications of these materials are listed in table 2.1. All rare earth doped $SrTiO_3$ systems are also mentioned in table 2.2.

Table 2.1: Specifications of the raw materials with their grades, purity and manufacturer used for preparation of various electro-ceramic samples.

S. No.	Raw Materials	Chemical Formula	Purity (%)	Manufacturer
1.	Strontium oxide	SrO	99.9	Alfa Aesar
2.	Titanium (IV) oxide	TiO_2	99.9	Alfa Aesar
3.	Lanthanum oxide	La_2O_3	99.9	Alfa Aesar
4.	Yttrium oxide	Y_2O_3	99.9	Alfa Aesar
5.	Samarium oxide	Sm_2O_3	99.8	Alfa Aesar
6.	Dysprosium oxide	Dy_2O_3	99.9	Alfa Aesar
7.	Titanium isopropoxide	$C_{12}H_{28}O_4Ti$	97.0	Alfa Aesar
8.	Ethylene glycol	$C_2H_6O_2$	99.0	Alfa Aesar
9.	Nitric acid	HNO_3	99.9	Alfa Aesar
10.	Citric acid	$C_6H_8O_7.\ H_2O$	99.9	Emplura

Table 2.2: Starting materials and firing schedule for various compositions.

S. No.	Composition	Starting Materials (A.R. Grade)	Calcination		Sintering	
			Temp. (°C)	Time (Hrs.)	Temp. (°C)	Time (Hrs.)
1.	$La_xSr_{1-x}TiO_3$	La_2O_3, SrO, TiO_2	1200	10	1400	12
2.	$Y_xSr_{1-x}TiO_3$	Y_2O_3, SrO, $C_{12}H_{28}O_4Ti$, $C_2H_6O_2$, HNO_3	1000	10	1200	12
3.	$Sm_xSr_{1-x}TiO_3$	Sm_2O_3, SrO, $C_{12}H_{28}O_4Ti$, $C_2H_6O_2$, HNO_3	1000	10	1200	12
4.	$Dy_xSr_{1-x}TiO_3$	Dy_2O_3, SrO, $C_{12}H_{28}O_4Ti$, $C_2H_6O_2$, HNO_3	1000	10	1200	12

2.3 Synthesis of Materials

2.3.1 Preparation of Nitrates

A few oxide materials (SrO, La_2O_3, Y_2O_3, Sm_2O_3 and Dy_2O_3) are prepared with standard nitrate solutions techniques. SrO powder material was dissolved in to dilute HNO_3 and solution was heated upto 100 °C until appearance of $Sr(NO_3)_2$ crystal. The weighted La_2O_3 was dissolved into dilute nitric acid to get $La(NO_3)_3$ homogenous solution. In addition $Y(NO_3)_3$, $Sm(NO_3)_3$ and $Dy(NO_3)_3$ solutions from Y_2O_3, Sm_2O_3 and Dy_2O_3 respectively, were carried out by the same procedure as mentioned for $Sr(NO_3)_2$ and $La(NO_3)_3$.

2.4 Synthesis Routes

In order to processing of materials two dissimilar synthesis routes were assumed. The schematic presentation of the two routes is shown in fig. 2.1.

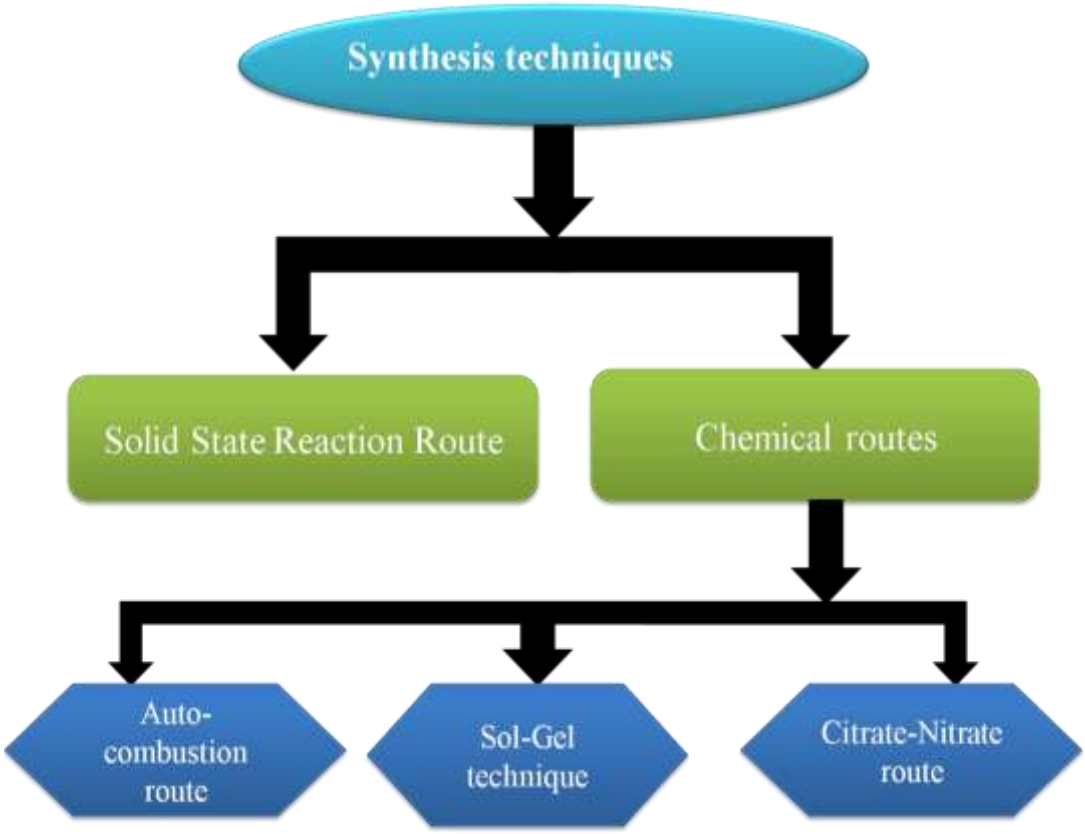

Figure 2.1: Block diagram of various synthesis techniques.

2.4.1 Solid State Reaction Route

Solid-state reaction technique is the most widely used method to synthesize the polycrystalline solids from a mixture of constituent solid oxides as starting materials. It should be careful that solid oxides should not react at room temperature. Primarily, high purity raw materials (constituent oxides) in powder form are first weighed according to their stoichiometric formula of the composition. The constituent oxides are mixed with an appropriate weighed amount and grounded with mortar pestle for homogenous mixing. The mixed reactants have been brought and play with volatile organic liquids like acetone/alcohol for homogeneity of compositions. For further mixing a ball mill is employed for mechanical mixing process with desirable operating and time rate. The required phase formation is investigated after calcination temperatures and loaded long holding time for sintering. All steps of solid state reaction method are shown in fig. 2.2. The series of perovskite system $La_xSr_{1-x}TiO_{3-\delta}$ at various doping percentage was synthesized through solid state reaction route.

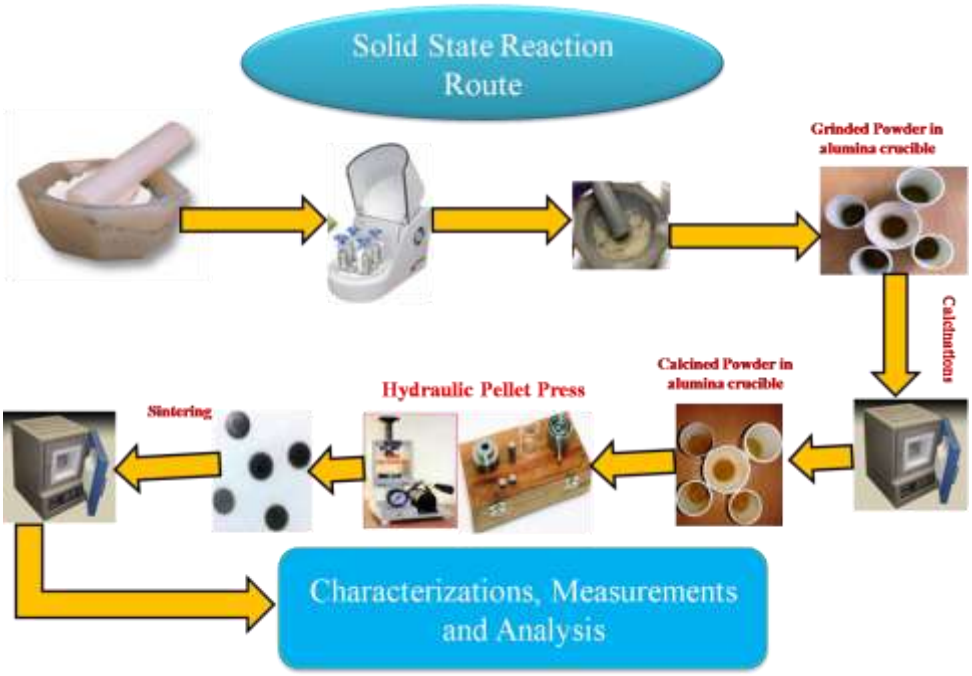

Figure 2.2: The image diagram representing the steps of solid state reaction method.

2.4.2 Chemical Reaction Routes

The chemical reaction route mechanism is fully-automated reaction techniques for all important reactions follow the complex chemical reactions. This is mainly for controlling and reducing the particle size and other relevant purposes to change chemical and physical properties of used materials. Their practical handling for systematic prediction has been also discussed in this chapter. Here we have used more than one independent complex chemical reaction methods: auto-combustion route, Sol-gel technique and citrate nitrate auto-combustion routes. Mostly nitrate materials were used for all chemical routes. In another process, few oxides were used as nitrates after converting into nitrates with dissolving them into dilute nitric acid. In this method, we have presented an overview of the chemical reaction routes, strategies and few results of applications to examine their practical handling for systematic prediction. The key stages in this route of sample preparation are calcination and sintering. The sintering condition was optimized at high temperatures to achieve the materials phase. The working steps of chemical reaction route are shown in fig. 2.3.

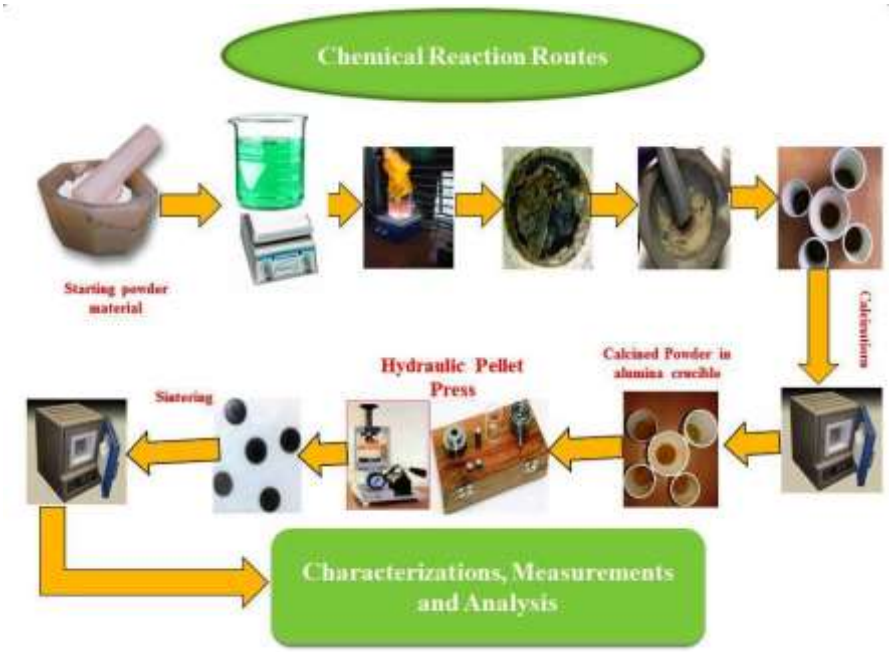

Figure 2.3: Diagram representation of chemical reaction route with the appropriate steps.

2.4.2.1 Auto-Combustion Route

Auto-combustion synthesis route has already been proposed in the study of many solid-state materials. It is previously studied that the properties of perovskite systems are strongly influenced via the materials composition and microstructure, which are very sensitive to the synthesis techniques. In various synthesis techniques such as sol-gel auto-combustion is relatively simple and fast process technique. In this process, high temperatures are attained in a short duration of a self-generated heat of reaction, yielding nanomaterials or loose agglomerates of nanocrystallites [79].

2.4.2.2 Sol-Gel Technique

The sol-gel technique has been applied to a variety of ceramic-perovskite systems ranging from room temperature to 200 °C. This method is relatively simple, fast and effective method to convert monomers into a colloidal solution that proceed to precursor solution. After drying precursor solution, a heating treatment was continued to get the better mechanical process, while structural stability such as densification and crystal grain growth as well as electrical property is achieved through a final sintering process [80]. Unlike to traditional processing methods, densification is frequently completed at much lower temperature from this method.

2.4.2.3 Citrate-Nitrate Auto-Combustion Synthesis

Citrate-Nitrate Combustion synthesis is an easy going and convenient technique for the preparation of several advanced electro-ceramics materials. However, citrate-nitrate auto-combustion synthesis process had previously been used for ceramic-perovskite systems. This synthesis technique is mainly utilized as a double function, citric acid as a fuel and metal nitrates are employed as metal and oxidant source [81]. The series of ceramic-perovskite systems $R_xSr_{1-x}TiO_{3-\delta}$ (R = Y, Sm and Dy) at various doping percentage was synthesized through citrate-nitrate auto-combustion route. All desired

nitrate precursors and citric acid were fully dissolved in distilled water to prepare the transparent homogenous solution. Furthermore, all prepared solutions were mixed together for homogeneity. To maintain the desired pH value between 1 and 4, a few drops of ammonia solution (40 wt. %) were added to resultant solution. Finally, the resulting mixture solution was slowly evaporated on a hot plate having temperature 200 ºC using magnetic stirrer. After the passes of time, a solution become gelled, foamed swelled and finally combusted. During evaporation, the solution was getting to change into the gel of nitrate mixture and that nitrate mixture was slowly formed as swelled and auto-ignite violently. After self-ignition a dried ash formed powder was obtained. The obtained powder was ground using mortar and pestle for further necessary characterization techniques.

2.5 Characterizations Techniques

This section describes the instruments/techniques employed for structural and electrical characterizations of all the prepared samples. A brief theoretical description of various characterizations techniques as XRD (X-ray powder diffraction), FESEM (Field emission scanning electron microscopy), XPS (X-ray photoelectron spectroscopy) and impedance spectroscopy are presented here. The block diagram of all above characterization and analyses techniques is shown in fig.2.4.

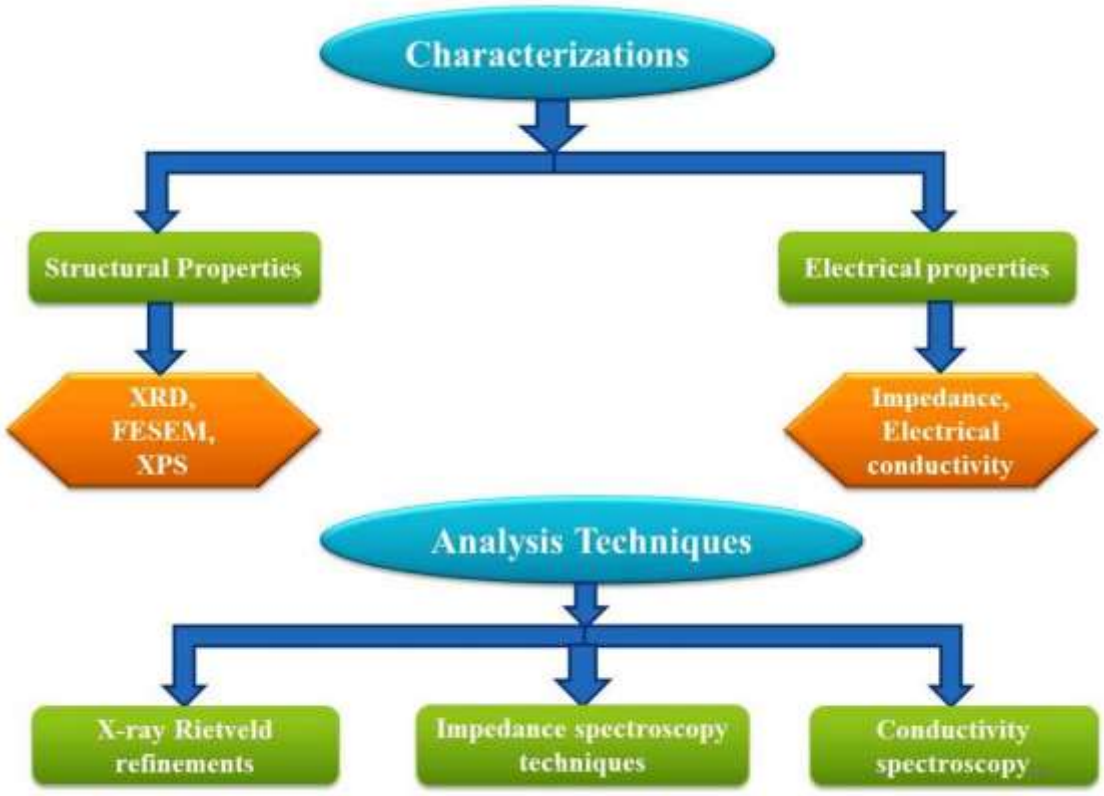

Figure 2.4: Block diagram of various Characterizations and analysis techniques.

2.5.1 Phase Formation and Crystal Structure Studies by Powder X-Ray Diffraction

A primary utilization of the X-Ray technique is phase identification and characterization of optimize materials to show their diffraction pattern. X-ray diffraction (XRD) shows dual wave/particle nature of X-rays to attain information about the crystal structure of materials. X-ray crystallography is a tool that measures the angles and intensities of diffracted beams to observe three-dimensional image of the density of electrons contained by the crystal. X-ray radiations are generally emitted by copper element along with its characteristic wavelength for the Cu-K_α radiation (λ = 1.54098 Å). When the incident beam targets a powder sample, sample and detector are rotated in 2θ orientation and diffraction peaks are recorded in term of intensity. The X-ray diffraction profile is used to determine the atomic arrangements in the materials because the inter-

planar spacing (d) of the diffracting planes is of the order of X-ray wavelength λ. For a crystal of given inter-planar spacing (d) and wavelength λ, the various orders n of reflection occurs only at a precise angle θ, which satisfies the Bragg condition: $2d\ sin\theta\ =\ n\lambda$ is shown in fig.2.5.

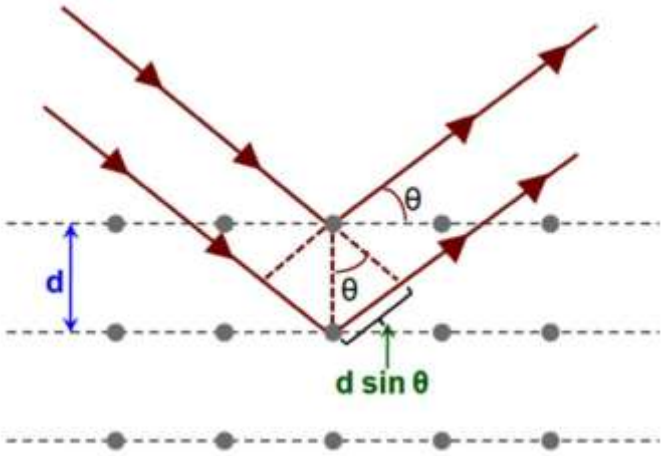

Figure 2.5: Schematic diagram of Bragg's law occurring through a crystal lattice [www.researchgate.net].

The mean positions of atoms in the crystal as well as their chemical bonds (bond angle, bond length), crystallite size, microstrain and various other information can be determined from the XRD pattern. In the x-ray system operation, the counter is arranged to scan over a range of 2θ values along with constant angular velocity. The basic principle of X-ray diffraction is to investigate the structural, physical and chemical information of the studied material. The single or multiple phase identification of an unknown material is the most important application of X-ray powder diffractometer. Moreover, the phase detection also supports to understand mechanism of formation of these materials and reveals its specific details. A powder diffraction technique has played an important role into structural physics, materials science and chemistry in determining the crystal structure of a solid into both organic and inorganic types. The X-ray measurement setup with working diagram is shown in fig. 2.6. In the present study, to confirm the single phase formation, powder XRD was done at different stages (i.e. as self-ignited ash,

calcined and sintered) of synthesis and processing of prepared samples. The obtained voluminous powder was ground using mortar and pestle calcined and sintered pellets was reground to observe powder X-ray diffraction patterns that were recorded using an X-ray diffractometer (Rigaku, MiniFlex 600) employing Cu-Kα_1 radiation with Ni filter. The single-phase formation of the solid solution was authenticated by the absence of characteristic lines of constituent oxides or any other phase between them in the XRD patterns also observed. The XRD patterns were indexed via JCPDS cards of PCPDFWIN program and lattice parameters were also determined using least square fitting of the recorded data using a software 'unit cell' program.

The average crystallite size and microstrain were calculated from XRD results by using Williamson-Hall model [82] given by the equation.

$$\beta cos\theta = 0.9\frac{\lambda}{t} + 4 \in sin\theta \tag{2.1}$$

where *t* is the average crystallite size, ∈ is the microstrain, β is the full width half maxima (FWHM) at Bragg's angle (2θ) and λ being the X-ray wavelength of Cu-K$_\alpha$. The slope of βcosθ vs. 4sinθ curve gives the value of microstrain and intercept gives the value of average crystallite size.

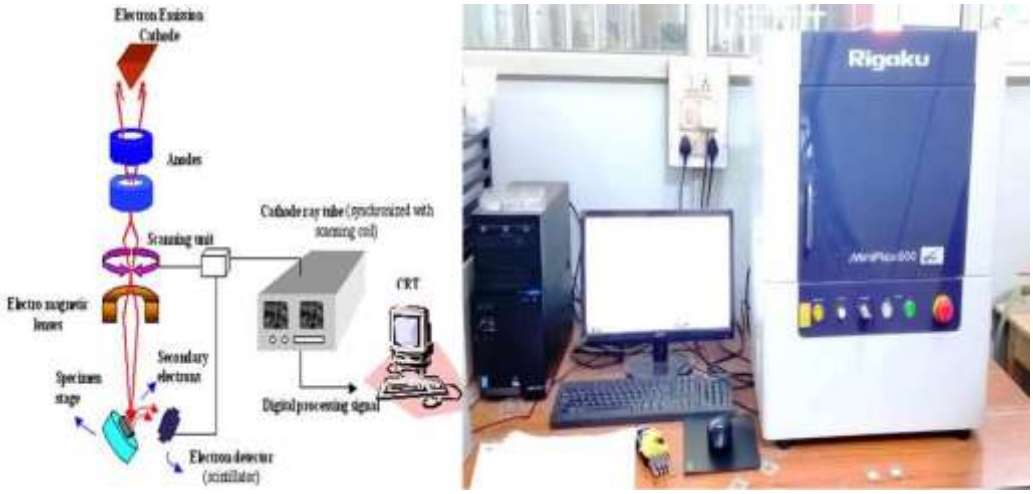

Figure 2.6: The construction of X-ray diffractometer with image of Rigaku (Miniflex 600) X-ray diffractometer.

2.5.2 Density and Porosity Measurements

There are various manual and automated techniques to determine experimental densities of the sintered pellets. In this chapter however, experimental densities was measured by Archimedes principle using water as a liquid medium. This method is both economically viable as well as time saving. The density measurement kit (Denver SI-234) is shown in fig. 2.7. Theoretical density was calculated from the molecular weight of the given compound and lattice parameters applying relation

$$\mathrm{D}_{th} = \frac{n \times M}{N \times V} \qquad (2.2)$$

where D_{th}, n, M, N and V are theoretical density, number of formula unit per unit cell, molecular weight of given sample, Avogadro's Number and unit cell volume, respectively. The standard method for percentage porosity was directly calculated using the relation

$$\%\, porosity = \left(\frac{D_{th} - D_{exp}}{D_{th}}\right) \times 100 \qquad (2.3)$$

where D_{th} and D_{exp} are given as theoretical and experimental densities.

Figure 2.7: The density measurement kit (Denver SI-234).

2.5.3 Microstructural Studies by Field Emission Scanning Electron Microscopy (FESEM) and Electron Dispersion Spectroscopy (EDS)

FESEM (Field Emission Scanning Electron Microscope) is the most important technique to examine the microstructure of studied compositions using focused electron beam on target materials. A cathode electron gun of a scanning electron microscope provides finer probing beams at low and high electron energy to improve the resolution and minimize the sample charging and damage. In vacuum atmosphere, electrons generated by a field emission source, are accelerated under a field gradient. The applied electron beam scanned microstructure images and detected which contains the information about the sample's surface. To optimize the microstructure, samples must be electrically conductive at the surface and electrically grounded to prevent the accumulation of electrostatic charge at the surface. In the most common scanning electron microscope, a detector catches the secondary electrons that are emitted by atoms excited by the electron beam. Finally, the micrograph images are displayed on a monitor. FESEM makes clearer images and less electrostatically distorted images with resolution upto 1-2 nm. EDS (Energy dispersive spectroscopy) is generally attached with FESEM, which provides elemental information with peak reflection in energy distribution curve of characterise materials. The atomic number of content element should be greater than boron and concentrations of detectable element at least order of 0.1 % to identify the elemental composition of materials. The high-resolution FESEM permits the study of very fine microstructural information and surface morphology analysis (Particles shape and size) such as grain orientation, texture and phase detection, fractured analysis and interface behaviour as well as qualitative elemental analysis.

In order of FESEM characterization, sintered pellets were polished using emery papers of various grades as 1/0, 2/0, 3/0, 4/0 and 5/0 (Sia, Switzerland) sequentially after

that these were chemically etched. The surface morphology was recorded using, field emission scanning electron microscope (NOVA NANOSEM 450). A field emission scanning electron microscope with EDS was used to test out the surface micrograph of the compositions as shown in fig. 2.8.

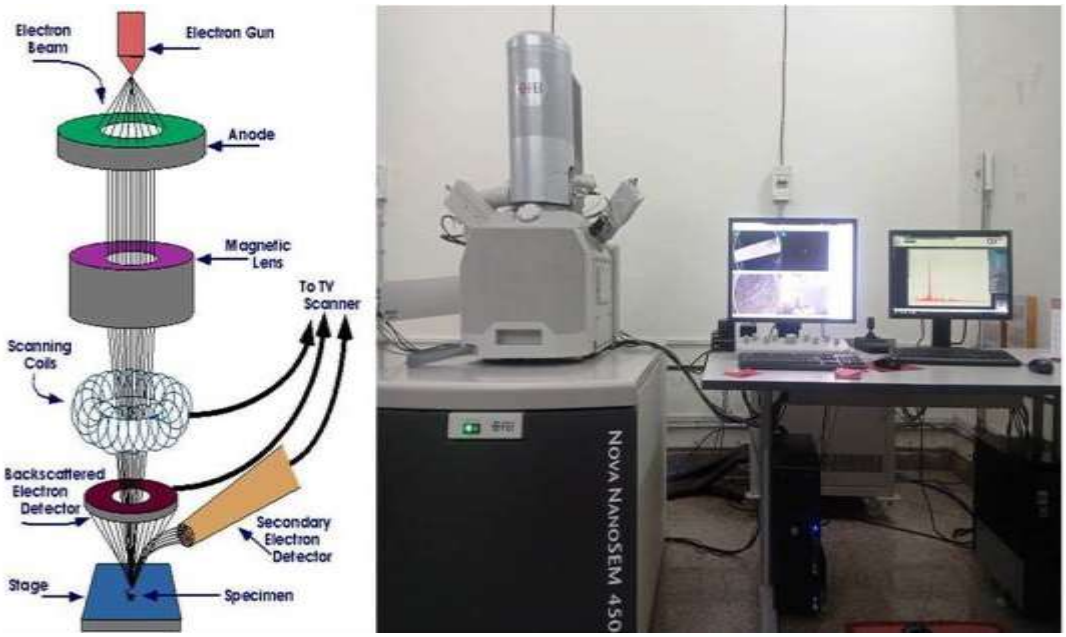

Figure 2.8: Schematic diagram of FESEM with image of FEI (NOVA NANOSEM 450).

2.5.4 X-ray Photoelectron Spectroscopy

XPS (X-ray photoelectron spectroscopy) is the most widely used surface analysis technique to study the surface chemistry of a material of each element and their chemical states and electronic states that exist within a material. XPS analysis does not only provide the presence elemental, but also detects the binding energy of emitted electrons which can provide chemical bonding information. Excited electrons are emitted from the parent atom as photoelectrons if their binding energy is lower than the X-ray energy. Each element possess a characteristic peak of binding energy that is indicated in a binding spectrum by analyser with the corresponding electron configuration of the atoms like 1*s*, 2*s*, 2*p*, 3*s*, etc. The number of detected electrons in each of the characteristic peaks is

directly related to the amount of element within the XPS sampling volume. In basic principle, the energies of the photoelectric lines are well described in terms of the binding energy of the electronic states of atoms (see fig. 2.9). The chemical states of the atoms at the surface result are in well-identified energy shifts to the peak energies. In the study of conducting samples, the detected electron energies can be referenced to the Fermi energy of the spectrometer; an absolute energy scale can be established for identification of species.

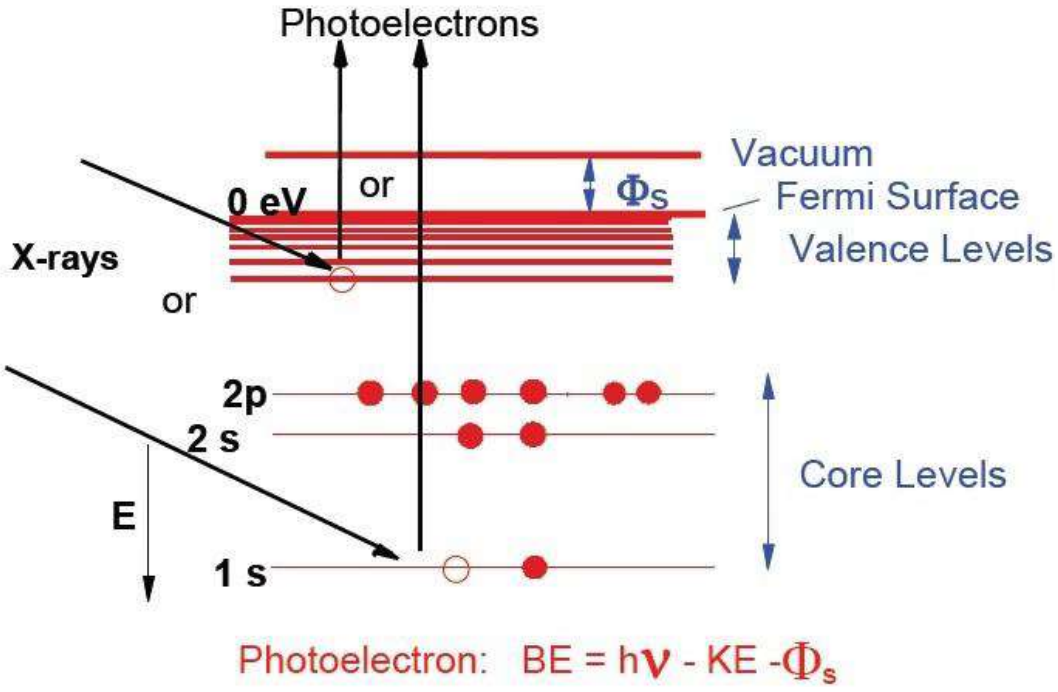

Figure 2.9: A Schematic diagram of XPS (X-ray photoelectron spectroscopy) [wiki.utep.edu].

In the present study, XPS analysis confirms the oxidation state of the different elements present in the studied samples. The obtained XPS spectrums corresponding to rare earth element (R), Sr, Ti, and O for the system $R_xSr_{1-x}TiO_3$ are schematically corrected with respect to C 1s peak appeared at 284.6 eV. An Amicus XPS setup was utilized to performed elemental analysis and chemical state of the given compositions as shown in fig. 2.10.

Figure 2.10: A Schematic design of XPS (X-ray photoelectron spectroscopy) working with photograph of XPS setup (KRATOS Amicus model).

2.6 Conductivity Measurement

2.6.1 Conductivity Measurement in Air using Impedance Analyser

Various methods have been suggested to measure the electrical conductivity. Among them two probes (ohmmeter or voltmeter–ammeter measurements) can be used for higher resistive samples and four probes methods (potential probe measurements) for the low resistive samples. Two probes measurement is the relatively simplest method of measuring conductivity. This method is practically useful when the sample has a large resistance. In this method, conductance is measured across the voltage drop V across the sample and current through the measured sample. The electrical measurement is investigated by sintered pellets which are polished with the help of emery papers of grade order 1/0, 2/0, 3/0, 4/0, 5/0 (Sia, Switzerland) and after that silver (Ag) paste was coated on both surfaces of the pellets. These coated pellets were cured at 700 °C for 20 minutes. The impedance measurements of the real and imaginary parts i.e. Z' and Z'' of different samples were carried out on silver coated electrodes pellets using two probe method in

the frequency range 20 Hz to 1 MHz and at an interval of 20 °C from room temperature to 700 °C in air using a Wayne Kerr 6500 P impedance analyser. AC impedance measurements were evaluated through PID controlled electric furnace along with sample holder. The measurement setup of Wayne Kerr 6500 P impedance analyser is shown in fig. 2.11.

Figure 2.11: Computer controlled automated impedance analyser setup along with sample holder and furnace (6500 P Wayne Kerr, UK).

2.6.2 Electrical Measurements in Reducing Atmosphere using Probostat

The electrical measurements in reducing atmosphere were carried out using the Probostat (Norecs, Norway) system. The Probostat system (fig. 2.12) permits to study the electrical properties of materials used for the manufacture of fuel cells, complete cells testing or its parts (cathode, electrolyte and anode). This instrument consists of assembled parts made of ceramic material (like alumina), which is suitable to resist high temperatures and that, given its inert nature, allows the use of various gases without the danger of unwanted reactions. This instrument is divided into two basic parts: the lower part and outer part. The lower part hexagon, which is made of steel and nickel-plated brass, has the function to accommodate the electrical and power connections and exhaust

of gas input and output from the device; the reaction section, made of alumina is characterized by an inner and an outer compartment and allows the housing and fastening of the sample.

Figure 2.12: The Probostat (Norecs, Norway) system impedance Analyser (FRA, mod. SOLARTRON 1250 - Schlumberger), in a range of frequency between 1-10^6 Hz.

The outer part is consisted with four Pt electrodes, connected by Pt wires to impedance meter to read the potential and the current, one thermocouple for a correct estimate of the sample temperature during the tests; a system of springs for mechanical load of samples: a tube used to seal the outer compartment. The impedance measurements could be done with electrochemical interface (EI, mod. 1286-Schlumberger) used in potentiostatic mode and connected to a Frequency Response Analyser (FRA, mod. SOLARTRON 1250-Schlumberger, fig. 2.12) in a range of frequency between 1-10^6 Hz.

2.7 Analysis Techniques

2.7.1 Phase Formation Study by Rietveld Refinement Technique

To determine the phase purity, crystal structure and lattice parameters, the Rietveld technique is more widely used. The Rietveld method along with a modelling of the peak profile is extremely useful for study of metastable and mixed phase form the studied materials. Due to an existence of crystal structural defects like dislocations, stacking faults, anti-phase domains, micro-strains and small crystallite sizes apparent in the diffraction pattern by a broadening of the Bragg peaks [82], [83]. Generally, the Voigt approximation for peak broadening is sufficient to acquire quantitative explanation of the presenting defects through the various lattice planes (*hkl*) and angular dependence of the peak broadening.

The Voigt approximation is based on the assumption that the convolution of the various effects has been found to result in a Gaussian shape. If this distribution is taken then the contribution of a given reflection to the profile y_i at position $2\theta_i$ is

$$y_i = I_k \exp\left[\frac{-4\ln(2)}{\beta_k^2}(2\theta_i - 2\theta_k)^2\right] \quad (2.4)$$

where β_k is the full-width half-maximum, $2\theta_k$ is the centre of the reflex, and I_k is the calculated intensity of the reflex that can be determined from the structure factor, Lorentz factor and multiplicity of the reflection. At very low diffraction angles the reflections could be attained an asymmetry which occurs due to the vertical divergence of the beam. Rietveld refinement also draws a semi-empirical correction factor,

$$A_s = 1 - \left[\frac{sP\,(2\theta_i - 2\theta_k)^2}{tan\theta_k}\right] \quad (2.5)$$

The width of the observed diffraction peaks are originated to broaden at higher Bragg angles. This angular dependency was originally represented in terms of FWHM parameters

$$\beta_k^2 = Utan^2\theta_k + Vtan\theta_k + W \quad (2.6)$$

where *U*, *V* and *W* are the FWHM parameters are refined during the peak fitting. The basic principle of the Rietveld refinement is to minimize a function *M* that can be analysed the difference between a calculated profile y^{cal} and the observed data y^{obs}.

$$M = \sum_i W_i \left(y_i^{obs} - \frac{1}{c} y_i^{cal}\right)^2 \quad (2.7)$$

where W_i is the statistical weight and c is an overall scale factor such that $y^{cal} = cy^{obs}$. FullProf program is suitable software to study the Rietveld refinement. This software has been basically developed for Rietveld analysis [84]–[87] (peak profile refinement) of neutron diffraction pattern (nuclear and magnetic scattering) or X-ray powder diffraction data refined at constant or variable step in scattering angle 2θ. In the current study, we give most of the information to the treatment of microstructural effect employing the FullProf program. The peak profiles were modelled by using pseudo-voigt function and back-ground has been described in terms of 6th coefficient polynomial. The R_{wp} (weighted-pattern factor), *R* values (R_p), χ^2 values and *S* (goodness-of-fit) parameters were used as numerical criterion of quality of the fit of calculated to experimental diffraction data. The structural parameters of the powders were investigated by the Rietveld analysis of XRD data applying the FullProf program.

2.7.2 Process of Analysing FESEM and XPS Study

The microstructural features of all rare earth doped $SrTiO_3$ systems were studied by field emission scanning electron microscope (FESEM) (Model: NOVA NANOSEM 450). The average grain size of all compositions was calculated by Image-J software using intercept method. After the microstructural analysis, Archimedes method was employed to confirm the density of all samples.

The XPS analyses were performed on high-performance analytical machine (KRATOS: Amicus) with magnesium target under 10^{-6} Pa pressure. The XPS spectrum of constituent elements was investigated under the range of 0-1150 eV with core and satellite binding energy peaks. The binding energy (BE) peaks of the constituent elements were corroborated for all compositions. The presence of a C-1s peak at ~286 eV may originate from external contamination. The binding energies were calculated after calibration with respect to the C-1s reference peak at ~284.6 eV. Thereafter, the XPS peaks of constituent elements were further analysed and fitted by XPSPEAK 4.1 software.

2.7.3 Electrical Properties

The electrical behaviours of the compositions were studied by following two techniques:

2.7.3.1 Conductivity Spectroscopic Technique

Electrical conductivity spectroscopy is a most useful technique to investigate electrochemical properties of the mixed conductors (ionic and electronic). The electrical conductivity is measured in two regimes dc and ac conductivity (σ_{dc} and σ_{ac} respectively). The dc conductivity of polycrystalline materials assumes only single dynamic response with frequency independent behaviours. Generally, conductivity measurements are operated with dc bias over the materials which show the polarization at the electrode/electrolyte interface of the material. In polycrystalline materials, electrical conductivity relaxation arises with contributions grain, grain boundary, and electrode-specimen interface. In case of electro-ceramics, frequency dependant conductivity spectra distinguish into two dispersion regime, low frequency regime (or frequency independent regime) plateau that represents dc conductivity while at high frequency, frequency dependent dispersive region represents ac conductivity. Both regions are attributed to combined effect of grain and grain boundary relaxation in absence of electrode

polarisation processes. The dc conductivity (σ_{dc}) of the system was evaluated from the low frequency plateau of the conductivity spectra and is shown in Arrhenius fashion which shows relatively low value due to electrode polarisation dominating at low frequencies. The conduction mechanism is studied in two parts: the frequency-independent part allotted to the dc conductivity which caused by the random motion of the mobile charge carriers, and the frequency-dependent part (dispersion regime) allotted to the ac conductivity (σ_{ac}) due the hopping motion of the mobile charge carriers in grains and grain boundaries [88]. In most polycrystalline ceramic materials the frequency dependent real part of the conductivity spectra is given by

$$\sigma' = \sigma_{dc} + \sigma_{ac} \tag{2.8}$$

where the ac conductivity (σ_{ac}) can be written with general formula

$$\sigma_{ac}\,(v, T) = A(T).\, v^{n(T)} \tag{2.9}$$

where *A* is a constant and also depends on various factors. The real part of electrical conductivity σ' can be described applying of Jonscher's power law.

$$\sigma' = \sigma_{dc}\left[1 + \left(\frac{v}{v_H}\right)^n\right] \tag{2.10}$$

where v_H parameter is the hopping frequency, v is the frequency and *n* is exponent factor that can be found to be less than 1. By the use of eq. (2.10), we can fit the conductivity spectra of the system as shown in fig. 2.13. The values of σ_{dc}, v_H and *n* can be easily estimated by fitting the conductivity spectra using Jonscher's power law.

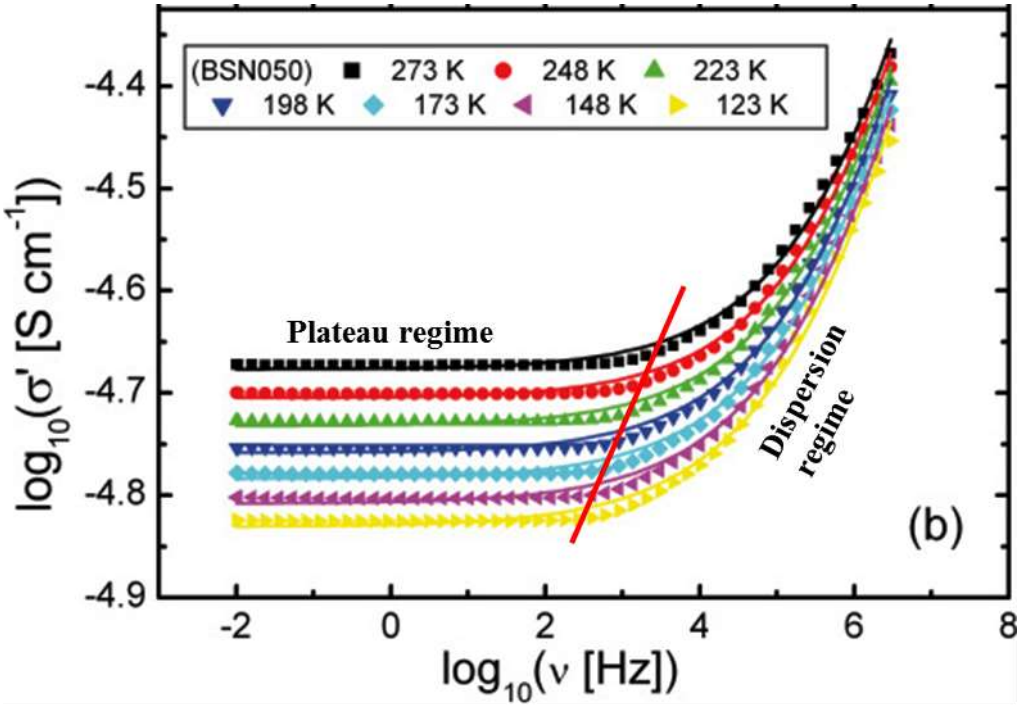

Figure 2.13: A typical conductivity spectra of a polycrystalline material [89].

2.7.3.2 Impedance Spectroscopic Technique

Impedance Spectroscopy (IS) is an effective and simple tool to study the electrical properties of the polycrystalline materials. It facilitates the tailoring of polycrystalline materials by separating out the contribution of different parts i.e. grain, grain boundary and electrode-specimen interface to the electrical conductivity. The electrical and dielectric properties of polycrystalline electronic ceramics have three contributions: grains or bulk, grain boundaries and electrode polarization interface. Impedance spectra are composed of three depressed semi-circular arcs which are characterised to grains or bulk, grain boundaries and electrode polarization, respectively. It is necessary to separate these contributions. Primarily, the observed difference in capacitances can be separated the contribution of observed semi-circular arcs. The capacitance corresponding to observed semi-circular arc was calculated by the relation $2\pi fRC$=1, where *f*, R and C are peak frequency, resistance and capacitance, respectively, which holds good at peak of the corresponding semi-circular arc.

Impedance study has emerged as a simple tool to separate the various contributions consists in the electrical/ dielectric properties of electronic ceramics [90], [91]. It is a functional tool to study defects, microstructure, surface chemistry and electrical conductivity of polycrystalline ceramic materials to explore a different kind of properties such as dielectrics, ionic conductors and adsorbate-adsorbent interface. The response of ac in the materials can be expressed by any of the four basic formalisms. These are complex impedance (Z^*), admittance (Y^*), electric modulus (M^*) and permittivity (ε^*) jointly referred to as spectroscopic functions which are expressed the following equations:

Complex impedance: $$Z^* = Z' - iZ'' = \frac{1}{i\omega C_0 \varepsilon^*} \quad (2.11)$$

Complex Admittance: $$Y'' = Y' + iY'' = i\omega C_0 \varepsilon^* \quad (2.12)$$

Complex modulus: $$M^* = M' + iM'' = \frac{1}{\varepsilon^*} \quad (2.13)$$

Complex permittivity: $$\varepsilon^* = \varepsilon' - i\varepsilon'' \quad (2.14)$$

Each is correlated among various parameters can be described as follows:

$$D = \tan\delta = \frac{\varepsilon''}{\varepsilon'} = \frac{M''}{M'} = \frac{Y'}{Y''} = \frac{Z'}{Z''} = \frac{\sigma'}{\sigma''} \quad (2.15)$$

$$Z' = \frac{D^2}{G \cdot (1 + D^2)} \text{ and } Z'' = \frac{Z'}{D} \quad (2.16)$$

$$\sigma' = \omega\varepsilon_0\varepsilon'' \text{ and } \sigma'' = \omega\varepsilon_0\varepsilon' \quad (2.17)$$

where ω is the angular frequency (ω=2πf) of applied electric field, f being the frequency in cycles/sec, C_0 is known as the geometrical capacitance. Z*, Y* and M* are generally used in the analysis of electrical/dielectric properties of electronic ceramics. These parameters are plotted in form of complex plane plots e.g. Z″ vs. Z′, M″ vs. M′ and spectroscopic plots Z″ or M″ vs. log ν. If electro-ceramics have the contributions of

grains, grain boundaries and electrode, then each of them can be represented by a circuit element diagram containing R and C connected in parallel. Therefore these are represented by an equivalent circuit containing three parallel RC circuit elements functioning in series as shown in fig. 2.14.

Nyquist plots (Cole-Cole plots) are usually plotted to explain frequency response information of a system by complex impedance function $Z^*(\omega) = Z'(\omega) - iZ''(\omega)$, where $Z'(\omega)$ and $Z''(\omega)$ are the real and imaginary parts of $Z^*(\omega)$. The real part of impedance (Z') and imaginary part (Z'') are defined as

$$Z' = \frac{R_g}{(1+\omega R_g C_g)^2} + \frac{R_{gb}}{(1+\omega R_{gb} C_{gb})^2} \tag{2.18}$$

$$Z'' = R_g \frac{\omega R_g C_{gb}}{(1+\omega R_g C_g)^2} + R_{gb} \frac{\omega R_{gb} C_{gb}}{(1+\omega R_{gb} C_{gb})^2} \tag{2.19}$$

where R_g and C_g are the bulk (grain) resistance and capacitance, respectively, and R_{gb} and C_{gb} are the corresponding quantities for interfacial boundary (grain boundary). The relative intercept position of the two semi-circular arcs in a complex plane can be identified by frequency. The arc of bulk indicates higher frequency than that of interfacial boundary since the relaxation time for the interfacial boundary is much larger than that for the bulk crystal. Therefore, when the bulk resistance (R_g) is much lower and the resistance in the equivalent circuit is led by the interfacial boundary resistance (R_{gb}), the arc of bulk (grain) may be in the limited frequency range. Resistance R_g, R_{gb} and R_{el} are symbolised the resistive contributions of grains, grain boundaries and electrode polarization process while C_g, C_{gb} and C_{el} symbolise their corresponding capacitive contributions, respectively. The analysis of complex plane impedance and modulus spectra are observed three semi-circular arcs with their intercepting on the real axis which have a single value of relaxation time as shown in fig. 2.14.

Relaxation time (τ) inversely proportional to angular frequency, ω at which the relaxation peak occurs, is given by the *RC* product.

$$\tau = 1/\omega = RC \tag{2.20}$$

N. Hirose and A. R. West were also reported the equations for the real axis intercepts for various immittance functions in complex plane plots [92].

The intercepts of the arcs on M′ axis in modulus plots are inversely proportional to the capacitance value (C_o/C_g, C_o/C_{gb} and C_o/C_{el}). The capacitance value from the impedance plots and resistance from the modulus plots can be observed from the peak frequency point in the arc by the relation $\omega RC = 1$. The entire measured frequency increases in opposite direction in complex plane impedance of modulus plots. The electrode polarization processes is very slow-moving that appear in the lowest frequency range followed by grain boundaries in the intermediate frequency range and bulk or grains contribution appears in the highest frequency range in the impedance spectra. The considerable number of arcs appearing in the complex plane plots which also depends on the ratio of various times constants. An electro-ceramics also having negligible value of electrode-interface contribution can be represented by two parallel RC elements connected in the series circuit. Grain and grain boundary conductivities σ_g and σ_{gb} could be determined using relations $\sigma_g = (1/R_g)\cdot(t/A)$ and $\sigma_{gb} = (R_gC_b / R_{gb}C_{gb}).\sigma_g$, respectively, with respective capacitances (C). These resistance and capacitance parameters (i.e. R_g, R_{gb}, C_g and C_{gb}) are satisfied the impedance tool from the best fit of the Nyquist plots at various temperatures.

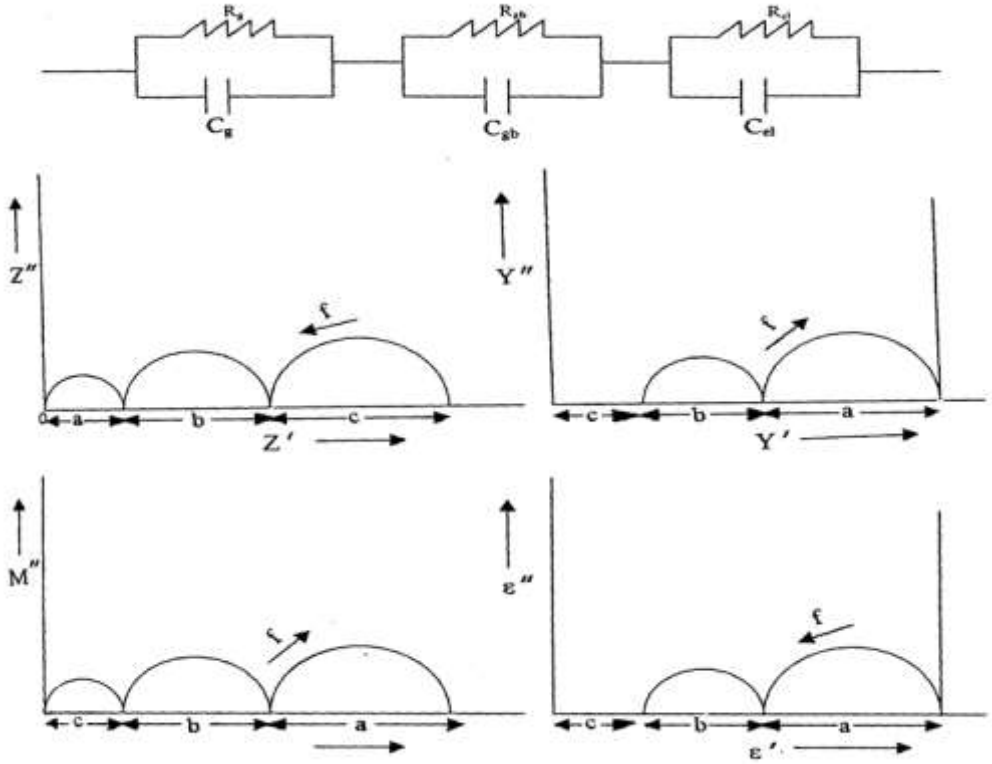

Figure 2.14: Equivalent circuit for a polycrystalline ceramic sample and corresponding frequency response in the Nyquist plots [93].